Int. J. Heat Mass Transfer. Vol. 35, No. 5, pp. 1261–1273, 1992
Printed in Great Britain

0017–9310/92 $5.00 + 0.00
© 1992 Pergamon Press Ltd

Thermohaline convection in a porous medium heated from below

N. D. ROSENBERG†
Department of Geological Sciences, University of California, Santa Barbara, CA 93106, U.S.A.

and

F. J. SPERA
Department of Geological Sciences and Institute for Crustal Studies, University of California, Santa Barbara, CA 93106, U.S.A.

(*Received* 25 *October* 1990 *and in final form* 1 *May* 1991)

Abstract—Results from numerical experiments of convection in porous media heated from below with two opposing sources of buoyancy (e.g. heat and salt) are presented. Steady-state calculations with a 'salted from below' boundary condition on composition and Dirichlet conditions on temperature in the region $100 < Ra < 600$, $10 < Le < 100$, $0 < R\rho < 0.4$ show that $Nu \propto Ra^{3/5}(1-R\rho)^{1/2}$ and $Sh \propto Ra^{3/5}Le^{1/2} \times (1-R\rho)^{1/2}$. Time-dependent simulations with $\phi^* = 1$ show that flows depend dramatically on $R\rho$ at constant Ra and Le. When the system is 'salted from below', the dynamics change with increasing $R\rho$ from a system which evolves to a well-mixed convective steady-state, to one in which flow is chaotic with large amplitude fluctuations in composition, and finally to one which evolves to a conductive steady-state. For an initially layered salinity field, vertically stacked convection cells may exist transiently; the interface between the layer is highly unsteady.

INTRODUCTION

NATURAL convection through porous media with a single buoyancy source has been studied exensively [1, 2]. Flows with two sources of buoyancy have received much less attention. As in studies in viscous fluids [3], the addition of a second source of buoyancy dramatically changes the dynamics of heat and mass transfer. Our interest is in natural hydrothermal systems such as those along the globe-encircling system of mid-ocean ridges, in which the two sources of buoyancy are heat and salinity [4]. Double-diffusive flows are also of interest with respect to contaminant transport in groundwater and exploitation of continental geothermal reservoirs [5, 6].

Two regimes of double-diffusive convection are commonly distinguished. When the faster diffusing component is destabilizing, as it is when stably stratified saltwater is heated from below, the system is in the diffusive regime. When the slower diffusing component is destabilizing, as is the case when cold fresh water is overlain by hot salty water, the system is in the finger regime. In this study, attention is focused on double-diffusive convection in the diffusive regime. Convection can occur in the diffusive regime even when the overall density gradient is stable and linear stability analysis predicts that infinitesimal disturbances will decay. This subcritical, finite-amplitude convection occurs because the diffusivity of the destabilizing component, in this case heat, is greater than the diffusivity of the stabilizing component, salt (i.e. $Le > 1$).

Much of the published work regarding double-diffusive convection in porous media concerns linear stability analyses [7–14]. There are several numerical studies of double-diffusive convection in porous media with horizontal temperature and composition gradients [15–17]. Trevisan and Bejan [18] studied heat and mass transfer at steady-state in porous media heated from below where the buoyancy effect was due entirely to temperature gradients (the passive mixing regime). Laboratory experiments of the diffusive regime include studies by Murray and Chen [19] who investigated the onset of thermohaline convection in a laboratory porous medium and Griffiths [20] who obtained values of heat and chemical fluxes through an interface between two layers with different initial temperatures and chemical concentrations. Trevisan and Bejan [21] recently reviewed the literature on double-diffusion convection in porous media.

In the first part of this paper, results from steady-state calculations of porous media heated and salted from below are presented in order to determine the effect of Ra, Le and $R\rho$ on Nu and Sh. Results from studies of time-dependent, finite-amplitude convective flows ($\phi^* = 1$) are then presented. It is shown that

† Address for correspondence: Earth and Environmental Sciences Division, Los Alamos National Laboratory, Los Alamos, NM 87545, U.S.A.

NOMENCLATURE

a_L	longitudinal dispersivity
a_T	transversal dispersivity
C	solute concentration (mass fraction solute in fluid)
c_p	heat capacity
ΔC	solute concentration difference in vertical direction
D	effective dispersion coefficient
$\mathbf{D}_h$	hydrodynamic dispersion coefficient
D^*_{mol}	molecular dispersion coefficient
$\mathbf{g}$	gravitational constant
H	height of porous medium
j	solute flux
k	permeability
KE	kinetic energy per unit mass fluid
$\dot{KE}$	time rate-of-change of KE
Le	Lewis number
Nu	Nusselt number
p	pressure
$\mathbf{q}$	Darcy velocity
q	heat flux
Ra	Rayleigh number
$R\rho$	buoyancy ratio
Sh	Sherwood number
T	temperature
t	time
ΔT	temperature difference in vertical direction
$\mathbf{v}$	fluid velocity ($\mathbf{q}/\sigma$)
x, z	Cartesian coordinate.

Greek symbols

α	coefficient of thermal expansivity
β	coefficient of chemical expansivity
δ_{ij}	Kronecker delta
κ	thermal diffusivity of saturated porous medium
μ	viscosity
ρ	fluid density
σ	heat capacity ratio, $\phi+(1-\phi)(\rho c_p)_{matrix}/(\rho c_p)_{fluid}$
ϕ	porosity
ϕ^*	ϕ/σ
ψ	streamfunction ($\partial\psi/\partial z = q_x$, $-\partial\psi/\partial x = q_z$).

Subscripts and superscripts

^	dimensionless variables
0	referenced to $\hat{z} = 0$.

flow dynamics depend strongly on $R\rho$ at fixed Ra, Le, and ϕ^* in a square domain for a variety of boundary and initial conditions on the salinity field and for Dirichlet conditions on temperature.

MATHEMATICAL FORMULATION

A two-dimensional equivalent porous medium that is homogeneous and isotropic is considered in this study. The equations governing double-diffusive convection in porous media include equations for the conservation of mass, momentum, energy, and species, and an equation of state for the fluid [22]. Conservation of fluid mass, assuming an incompressible fluid and no sources or sinks, can be expressed as

$$\nabla\cdot\mathbf{q} = 0. \tag{1}$$

Conservation of fluid momentum is expressed by Darcy's law, providing the fluid moves slowly so that inertial effects are negligible, as

$$\mathbf{q} = -\frac{k}{\mu}(\nabla p - \rho\mathbf{g}) \tag{2}$$

where k, the permeability, is isotropic and spatially invariant, and the fluid viscosity is taken as a constant.

Conservation of energy can be expressed as

$$\sigma\frac{\partial T}{\partial t} + \mathbf{q}\cdot\nabla T = \kappa\nabla^2 T \tag{3}$$

where it is assumed that the fluid and matrix are in thermal equilibrium and κ, the effective thermal diffusivity of the saturated medium, is constant.

Conservation of species can be expressed as

$$\phi\frac{\partial C}{\partial t} + \mathbf{q}\cdot\nabla C = \phi\mathbf{D}_h\nabla^2 C. \tag{4}$$

The coefficient of hydrodynamic dispersion, $\mathbf{D}_h$, is the sum of the coefficient of molecular diffusion in a porous medium, D^*_{mol}, and the coefficient of mechanical dispersion, $\mathbf{D}_{mech}$. D^*_{mol} is a scalar equal to the molecular diffusivity of solute in the fluid multiplied by the tortuosity of the medium. $\mathbf{D}_{mech}$ is a function of fluid velocity and medium characteristics and can be written

$$\mathbf{D}_{mech} = (a_L - a_T)\frac{v_i v_j}{|\mathbf{v}|} + a_T|\mathbf{v}|\delta_{ij} \tag{5}$$

where a_L and a_T represent the longitudinal and transversal dispersivities for an isotropic porous medium, δ_{ij} is the Kronecker delta and $|\mathbf{v}| = (v_x^2+v_z^2)^{1/2}$. The dispersivity coefficients a_L and a_T express the heterogeneity of the medium at the microscopic scale. In granular media, a_L is of the order of the grain size; in

fractured media, it is closely related to the average crack spacing. Transversal dispersivities are generally substantially smaller, often by factors of 5–100, than longitudinal ones. In writing equation (5), it is assumed that the dispersive flux of solute can be expressed in the Fickian form. In many practical circumstances, knowledge of the dispersivities is so meager that it becomes necessary to define an effective dispersion coefficient $D \equiv \phi \mathbf{D}_h$ which is taken as a constant scalar for the sake of simplicity. That practice has been adopted here so that attention can be focused on the role of chemical buoyancy ($\beta \Delta C$) in governing the global dynamics and not the details of dispersive transport. It is recognized, however, that an accurate and predictive model for double-diffusive convection in fractured porous media must eventually deal with the issue of anisotropy, both in permeability and dispersivity, in detail. Such studies are now in progress.

For the equation of state of the fluid, it is assumed that the fluid density is a function of temperature and concentration only

$$\rho = \rho_0[1-\alpha(T-T_0)+\beta(C-C_0)]. \tag{6}$$

All fluid and transport properties are assumed to be constant except for ρ in the body force term of the momentum equation (the Boussinesq approximation).

Equations (1)–(6) may be written in the following dimensionless form:

$$\nabla^2\hat{\psi} = -Ra\left(\frac{\partial \hat{T}}{\partial \hat{x}} - R\rho \frac{\partial \hat{C}}{\partial \hat{x}}\right) \tag{7}$$

$$\frac{\partial \hat{T}}{\partial \hat{t}} + \left(\frac{\partial \hat{\psi}}{\partial \hat{z}}\frac{\partial \hat{T}}{\partial \hat{x}} - \frac{\partial \hat{\psi}}{\partial \hat{x}}\frac{\partial \hat{T}}{\partial \hat{z}}\right) = \nabla^2 \hat{T} \tag{8}$$

$$\phi^* \frac{\partial \hat{C}}{\partial \hat{t}} + \left(\frac{\partial \hat{\psi}}{\partial \hat{z}}\frac{\partial \hat{C}}{\partial \hat{x}} - \frac{\partial \hat{\psi}}{\partial \hat{x}}\frac{\partial \hat{C}}{\partial \hat{z}}\right) = \frac{1}{Le}\nabla^2 \hat{C} \tag{9}$$

where ψ is the streamfunction ($q_x = \partial\psi/\partial z$, $q_z = -\partial\psi/\partial x$) and

$$\hat{x} = x/H, \quad \hat{z} = z/H, \quad \hat{t} = t\kappa/H^2\sigma$$
$$\hat{\psi} = \psi/\kappa, \quad \hat{T} = (T-T_0)/\Delta T, \quad \hat{C} = (C-C_0)/\Delta C. \tag{10}$$

The four dimensionless parameters governing the convective dynamics are the Rayleigh number (Ra), the Lewis number (Le), ϕ^*, and the buoyancy ratio ($R\rho$)

$$Ra = \frac{k\rho_0 \mathbf{g}_z \alpha \Delta T H}{\mu\kappa}, \quad Le = \frac{\kappa}{D}$$
$$\phi^* = \frac{\phi}{\sigma}, \quad R\rho = \frac{\beta \Delta C}{\alpha \Delta T}. \tag{11}$$

D is an effective dispersion coefficient equal to $\phi \mathbf{D}_h$ and is assumed to be a constant scalar.

The non-dimensional computational domain consists of a 1×1 box (Fig. 1(a)). The dimensionless boundary and initial conditions on $\hat{\psi}$ and $\hat{T}$ applicable to all of the simulations reported are

$$\hat{\psi} = 0, \quad \hat{T} = 1 \quad \text{at} \quad \hat{z} = 0$$
$$\hat{\psi} = 0, \quad \hat{T} = 0 \quad \text{at} \quad \hat{z} = 1$$
$$\hat{\psi} = 0, \quad \hat{q} = 0 \quad \text{at} \quad \hat{x} = 0, 1$$
$$\hat{\psi} = 0, \quad \hat{T} = 0 \quad \text{at} \quad \hat{t} = 0. \tag{12}$$

That is, the box has a hot bottom, a cold top and adiabatic sides. All walls are impermeable to flow and the fluid is initially cold and motionless.

Two sets of boundary conditions on $\hat{C}$ (Fig. 1(b)) have been studied. In the 'salted from below' case, the top and bottom walls are kept at a constant composition and no salt is allowed to leave the box through the wide walls,

$$\hat{C} = 1 \quad \text{at} \quad \hat{z} = 0$$
$$\hat{C} = 0 \quad \text{at} \quad \hat{z} = 1$$
$$\hat{j} = 0 \quad \text{at} \quad \hat{x} = 0, 1. \tag{13a}$$

In the 'no flux' case, zero flux boundary conditions on $\hat{C}$ along each wall are imposed. That is, no solute is allowed to enter or leave the domain,

$$\hat{j} = 0 \quad \text{at} \quad \hat{x} = 0, 1 \quad \text{and} \quad \hat{z} = 0, 1. \tag{13b}$$

Three sets of initial conditions on $\hat{C}$ (Fig. 1(c)) are considered: the 'empty box' case for which

$$\hat{C} = 0 \quad \text{for all } \hat{x} \text{ and } \hat{z} \text{ at } \hat{t} = 0 \tag{14a}$$

the 'layered box' case with two horizontal layers of different composition,

$$\hat{C} = 1 \quad \text{for} \quad \hat{z} < 0.5 \quad \text{at} \quad \hat{t} = 0$$
$$\hat{C} = 0 \quad \text{for} \quad \hat{z} > 0.5 \quad \text{at} \quad t = 0 \tag{14b}$$

and the 'linear box' case where $\hat{C}$ varies linearly from $\hat{C} = 1$ on the bottom wall to $\hat{C} = 0$ on the top wall,

$$\hat{C} = 1 - \hat{z} \quad \text{at} \quad \hat{t} = 0. \tag{14c}$$

At each time step, the flow, temperature and salinity fields are used to compute the spatially-averaged kinetic energy per unit mass of fluid (KE), the Nusselt number (Nu) and the Sherwood number (Sh). KE, a convenient measure of the vigor of the flow, is defined as

$$KE = \frac{1}{2}\int_0^1 \int_0^1 \left[\left(\frac{\partial \hat{\psi}}{\partial \hat{z}}\right)^2 + \left(\frac{\partial \hat{\psi}}{\partial \hat{x}}\right)^2\right] d\hat{x}\, d\hat{z}. \tag{15}$$

Nu, the ratio of the total heat transferred to the heat transferred by conduction alone for the imposed ΔT, is defined as

$$Nu = -\int_0^1 \left(\frac{\partial \hat{T}}{\partial \hat{z}}\right)_{\hat{z}=1} d\hat{x}. \tag{16}$$

Finally, Sh, the ratio of the total solute transferred to the solute transferred by diffusion alone for the imposed ΔC, is defined as

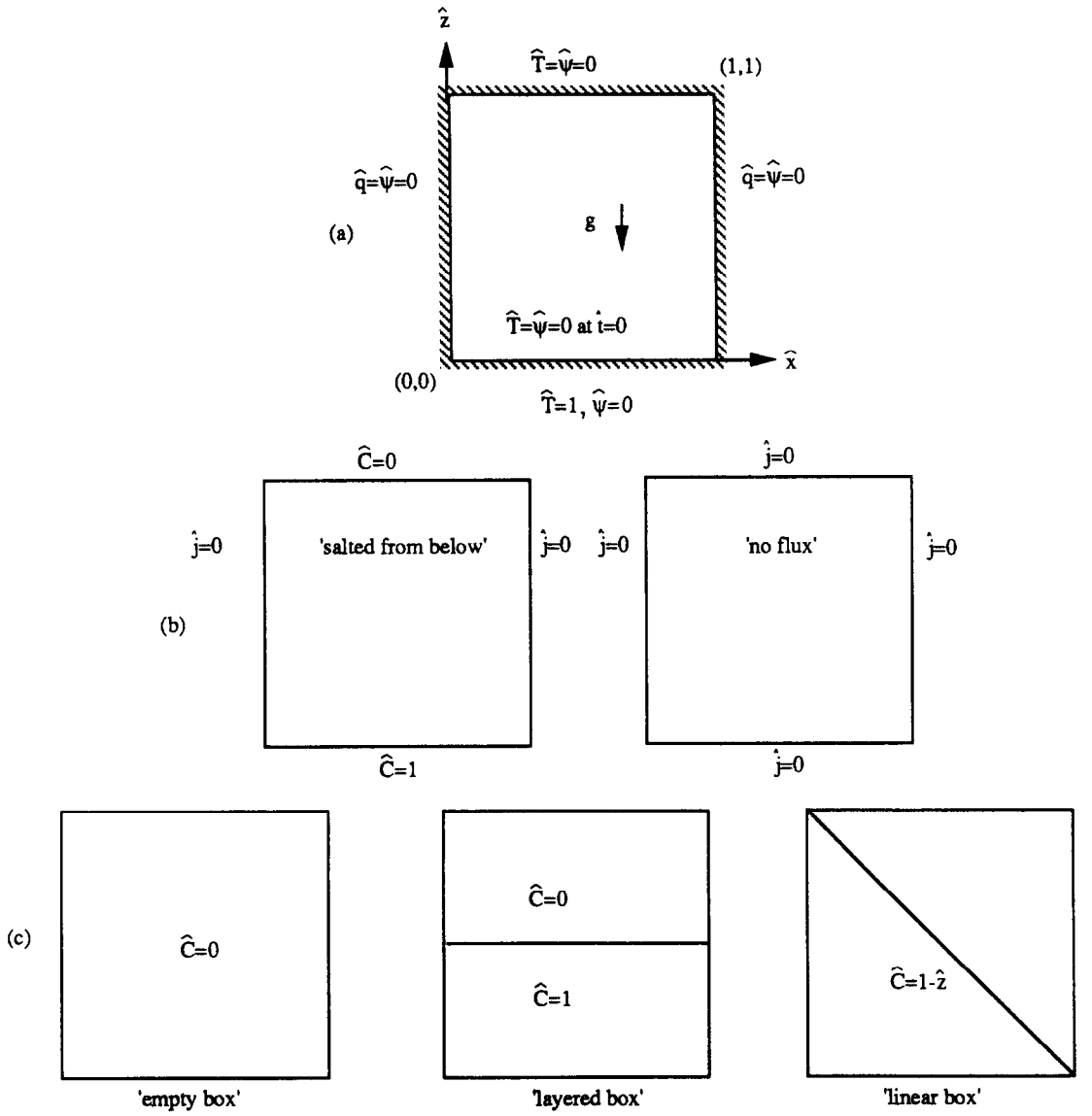

FIG. 1. (a) Domain, (b) boundary conditions, (c) initial conditions.

$$Sh = -\int_0^1 \left(\frac{\partial \hat{C}}{\partial \hat{z}}\right)_{\hat{z}=1} \mathrm{d}\hat{x}. \tag{17}$$

SOLUTION METHODOLOGY

Equations (7)–(9) are solved using a Galerkin finite element code used previously for other convection calculations [23, 24]; details of the method are given in ref. [25]. Briefly, triangular finite elements with quadratic basis functions are used to discretize the conservation equations and the resulting set of algebraic equations is solved by Newton–Raphson iteration. A fully implicit scheme is used to advance the energy and species equations forward in time. Validation of the code was accomplished by comparison with results from published numerical and laboratory experiments (Table 1 and Fig. 2).

A nonuniform grid of 1120 elements was used in the steady-state calculations. These calculations were all performed with the 'salted from below' boundary condition and the grid was graded so that the elements were concentrated in the boundary layers at the top and bottom of the domain. A comparison of KE, Nu and Sh values for various grids for parameters $Ra = 600$, $Le = 20$, $Rp = 0$ (Table 2) indicates that the solutions obtained with the 1120 element grid are accurate to within less than 1%. Note that Sh is much more sensitive to spatial resolution than either KE or Nu. KE is dominated by the higher velocities in the domain interior and is therefore insensitive to the

Table 1. Code validation against results from numerical experiments reported in the literature

	Nu		*Sh*		
	This study	Literature	This study	Literature	Ref.
$Ra = 50$, heated from below	1.5	1.5	—	—	[26]
$Ra = 600$, heated from below	6.6	6.6	—	—	[27]
$Ra = 50$, $Le = 10$, $R\rho = 0$, heated from the side	2.0	2.1	9.7	9.7	[15]
$Ra = 50$, $Le = 10$, $R\rho = 0.5$, heated from the side	2.0	2.1	15.0	15.0	[15]

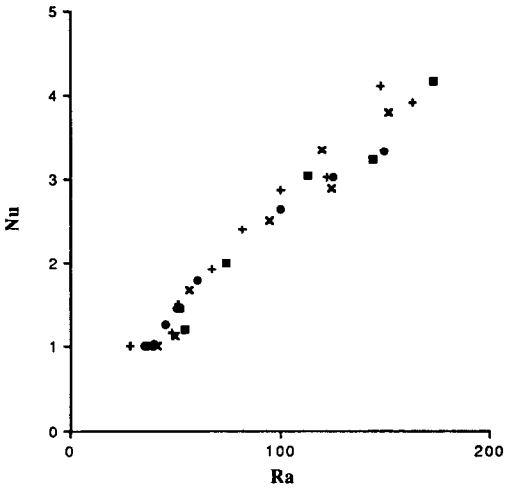

FIG. 2. Code validation. Numerical results using the code in the present study are plotted with results from laboratory experiments reported in the literature. • This study (aspect ratio of 1); × heptane and sand [28]; + water and glass beads [29]; ■ water and glass beads [30]. No aspect ratio was given for the three published studies referenced here and the values for *Ra* and *Nu* were read off published graphs. Note the excellent agreement between the numerical and the laboratory data.

exact thickness of the boundary layers. *Nu*, which measures the thickness of the thermal boundary layers, shows some sensitivity to spatial resolution. *Sh*, however, a function of the much thinner chemical boundary layers, is very sensitive to spatial resolution. Elementary scaling indicates that $Sh/Nu = Le^{1/2}$ and this relationship is verified in these calculations (Table 2).

Time-dependent results were obtained using both uniform grids of 800 elements and graded grids with 1120 elements and time steps on the order of 10^{-4}–10^{-5}. Additional calculations with finer spatial and temporal resolution were performed to verify the accuracy of the solutions. For the 'salted from below' boundary condition, simulations using 800 uniform elements overestimate the thickness of the chemical boundary layers at the top and bottom of the domain. However, major features predicted by the 800 element grid do not appear to change when a finer grid is used. In the example illustrated in Fig. 3, values for *Sh*, essentially a measure of the chemical boundary layer thickness, are underestimated by about 20%. The flow and temperature fields and the composition field in the flow interior, however, are well-resolved, with *KE* and *Nu* values accurate to within a few percent. Therefore, in some cases, the great additional computational expense associated with achieving grid independence was not believed to be justified. The resolution question is more difficult for chaotic flow solutions because, by definition, chaotic flows are highly sensitive to small differences in variable values and therefore to small differences in resolution. Simulations of flows performed at a variety of spatial and temporal resolutions suggest that the chaotic flows reported here are indeed chaotic, as evidenced by the fact that running average *KE*, *Nu* and *Sh* values and the broadband character of the corresponding power spectra are preserved.

RESULTS

In the following sections, the results of the numerical simulations are presented. The steady-state results are presented first, followed by discussion of the time-

Table 2. Spatial resolution comparison for steady-state calculations ($Ra = 600$, $Le = 20$, $R\rho = 0$)

Number of finite elements	Grid	*KE*	*Nu*	*Sh*	*Sh*/*Nu*†
800	uniform	1689	6.84	27.3	3.99
1000	graded	1691	6.65	30.4	4.57
1120	graded	1691	6.64	29.7	4.57
1600	uniform	1690	6.76	29.3	4.33
1760	graded	1690	6.64	29.9	4.50
2240	graded	1690	6.64	29.6	4.46
3200	uniform	1690	6.70	31.6	4.72
6400	uniform	1690	6.67	31.4	4.71

† Elementary scaling analysis predicts that $Sh/Nu \approx (Le)^{1/2}$, which in this case is $(20)^{1/2} \approx 4.47$.

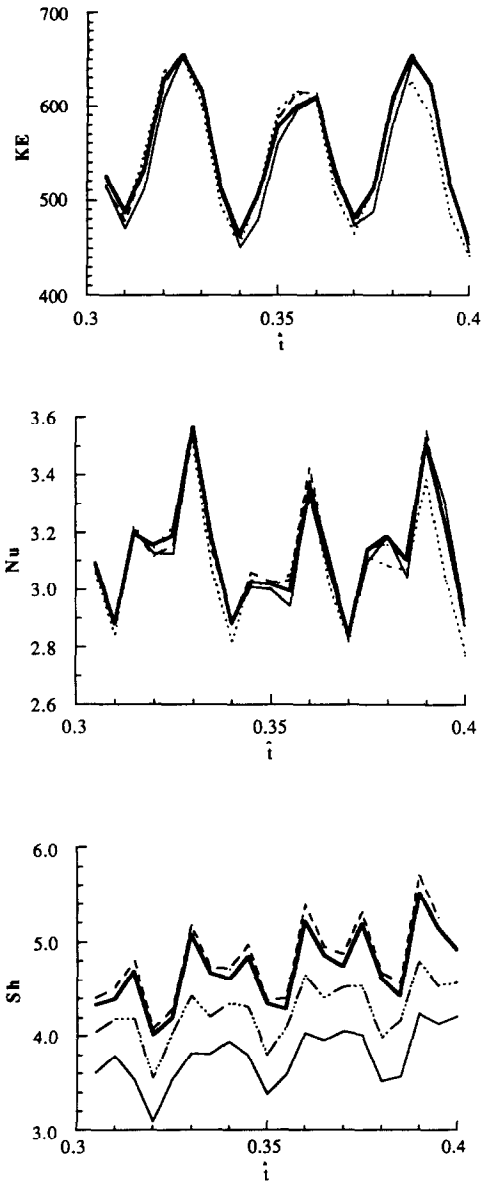

FIG. 3. Code verification. Kinetic energy (KE), Nusselt number (Nu) and Sherwood number (Sh) vs time for porous media heated from below with the 'salted from below' boundary condition and 'empty box' initial condition on composition. The parameters of this problem are $Ra = 600$, $Le = 20$, $\phi^* = 1$, and $R\rho = 1$. The various lines represent different spatial resolution: (——) 800 elements on a uniform grid; (— · · —) 1600 elements on a uniform grid; (- - -) 1120 elements on a graded grid with elements concentrated near the top and bottom walls; and (——) 2240 elements also on a graded grid. Note that Ke and Nu change $<1\%$ among the various grids. Sh values, however, are underestimated by the 800 element grid by $\sim 20\%$.

dependent calculations. Since the primary interest here is in the effect of the ratio of chemical to thermal buoyancy, $R\rho$, constant values are used for the other dimensionless parameters in the time-dependent simulations: $Ra = 600$ and $Le = 20$ and $\phi^* = 1$.

Steady-state

A series of steady-state calculations for a porous medium heated from below was performed to determine the effect of Le and $R\rho$ on Nu and Sh. Note that the term ϕ^* is not an explicit parameter in the steady-state problem. (The permeability and D, of course, depend on the porosity, ϕ). For the 'salted from below' boundary condition on the salinity field, 36 convective steady-state solutions were obtained in the range $100 < Ra < 600$, $10 < Le < 100$ and $0 < R\rho < 0.4$. At $Ra = 100$, the planform consisted of a single convection cell. For $Ra = 150$ and $Ra = 300$, the steady-state solution consisted of two side-by-side convection cells. For $Ra = 600$, a four-cell planform was obtained. Although a detailed study of steady vs unsteady regimes for this problem was not performed, in general, convective steady-state solutions did not exist at higher $R\rho$ values. The steady-state results are given in Figs. 4 and 5.

Figure 4(a) shows a plot of Nu vs Le at $R\rho = 0.2$ for different Ra values. These results show that Nu is essentially independent of Le. Obviously, at low $R\rho$ the flow field is determined by the transfer of heat, not solute; the solute behaves as a nearly passive tracer. However, the thickness of the chemical boundary layer, and hence Sh, does depend on Le. A plot of Sh vs Le (Fig. 4(b)) shows that Sh increases (i.e. the chemical boundary layer becomes increasingly thinner) with increasing Le. The effect of $R\rho$ on Nu and Sh is shown in Figs. 5(a) and (b). These plots show that Nu and Sh both decrease with increasing $R\rho$ for a given Ra and Le.

Regression analyses of the results shown in Figs. 4 and 5 leads to the parametric relationships $Nu \propto Ra^{3.5}(1 - R\rho)^{1.2}$ and $Sh \propto Ra^{3.5}Le^{1.2}(1 - R\rho)^{1.2}$ (with the correlation coefficient equal to greater than 0.99). These results agree well with those of Trevisan and Bejan [18]. These authors summarize the various relationships between Nu and Ra reported in the literature and from their own work for pure thermal convection; all fall in the range $Nu \propto Ra^n$ where $0.5 < n < 1$. They also report $Sh \propto Ra^{7.8}Le^{1.2}$ based on scaling analyses and numerical experiments for combined heat and mass transfer in the passive mixing ($R\rho = 0$) case.

For the 'no flux' boundary condition, it is always possible to obtain a convective steady-state solution that is a function of Ra and is completely independent of $R\rho$ and Le. The salinity field is homogeneous in the steady-state. The second law of thermodynamics for a binary fluid with no Soret or DuFour processes dictates that the composition must eventually homogenize.

Time-dependent—'salted from below' 'Empty-box'. Time-dependent simulations with $R\rho$ ranging from 0 to 3 were obtained for the 'salted from below' boundary condition and the 'empty box' initial condition. For $R\rho = 0$, corresponding to the problem of pure thermal convection with a passive tracer, the

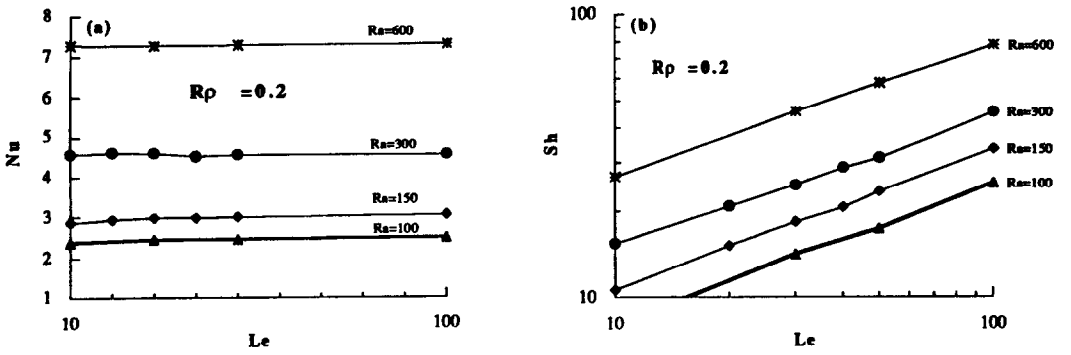

FIG. 4. (a) *Nu* vs Lewis number (*Le*) and (b) *Sh* vs *Le* at steady-state for the 'salted from below' boundary condition on composition. Calculations were performed for $R\rho = 0.2$ and a range of Rayleigh numbers (*Ra*).

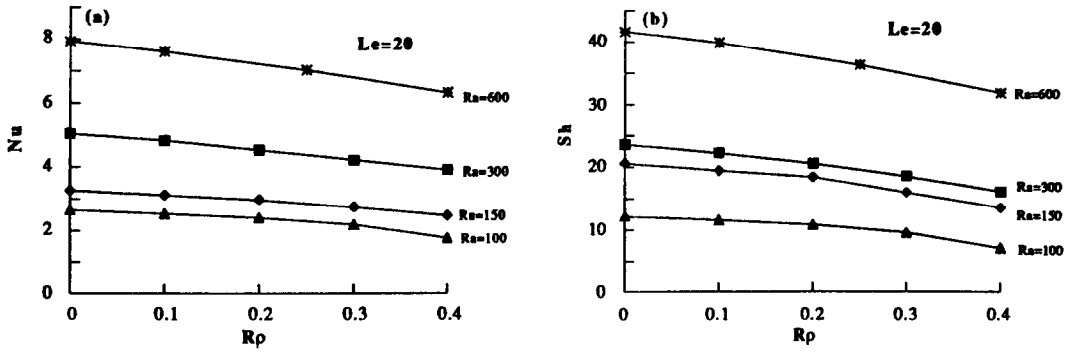

FIG. 5. (a) *Nu* vs buoyancy ratio ($R\rho$) and (b) *Sh* vs $R\rho$ at steady-state for the 'salted from below' boundary condition on composition. Calculations were performed for $Le = 20$ and a range of Rayleigh numbers (*Ra*).

flow and temperature fields rapidly ($\hat{t} \approx 0.11$) reach a convective steady-state consisting of two side-by-side convection cells elongated in the vertical direction. The steady-state velocity, temperature and concentration fields for $R\rho = 0$ are shown in Fig. 6. The flow consists of rising hot fluid, with a high solute concentration, in the center of the domain and colder fluid, with a lower solute concentration, sinking along the adiabatic and impermeable side walls. Thin temperature and much thinner composition boundary layers are found at the top and bottom of the domain and the interior is well-mixed and nearly homogeneous.

Nu vs time plots for six of these simulations are given in Fig. 7. At early time, each of these plots shows several large spikes which correspond physically to the transient associated with the onset of convection from the quiescent initial state. For the passive tracer and low $R\rho$ values, the systems evolve to a convective steady-state. At intermediate $R\rho$ values, the systems remain unsteady and at high $R\rho$ values, the system evolves toward a conductive steady-state with $Nu = 1$.

For low $R\rho$ values, the systems evolve to a convective steady-state consisting of four side-by-side convection cells. The time taken to reach the steady-state increases roughly linearly with increasing $R\rho$. During the evolution to a convective steady-state, flow is oscillatory. The oscillations take the form of 'sloshing' between two planforms. In one planform, the two outside convection cells are wider at the top and the two inside cells are wider at the bottom. In the other, the reverse is true, the two outside cells are wider at the bottom and the two inside cells are wider at the top. Oscillatory flow is characteristic of double-diffusive convection [3]. A physical explanation for oscillatory flow is easily offered. As fluid is heated from below, it becomes less dense and begins to rise. As it rises, the fluid encounters a cooler and less saline environment. As heat diffuses faster than salt in this system, the fluid loses heat more rapidly than it loses salt. This cooler but salty fluid is denser than the surrounding fluid environment and the fluid sinks. As it sinks into the warmer, more saline fluid environment, the fluid heats up before it becomes much saltier, again owing to the different diffusivities of heat and salt in the system, and so the fluid becomes

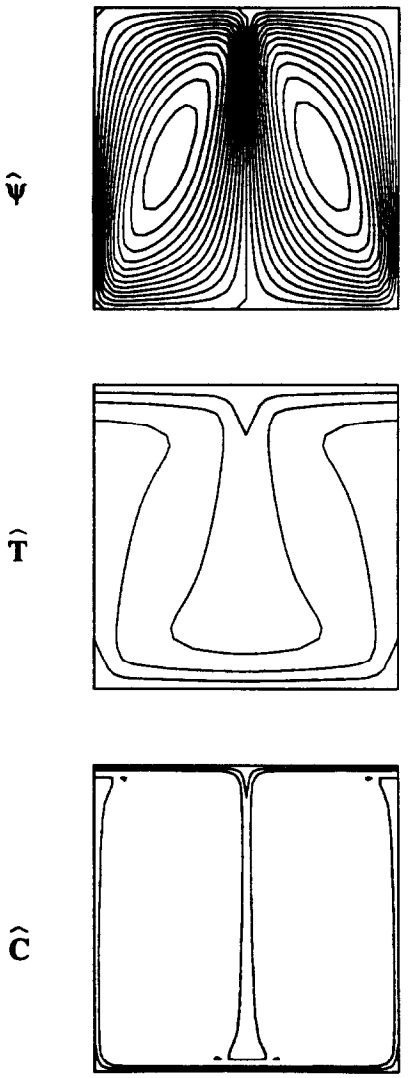

FIG. 6. Steady-state velocity, temperature, and composition field plots for passive tracer case (2-cell planform) with $Ra = 600$, $Le = 20$, $R\rho = 0$ and the 'salted from below' boundary condition. A graded grid with 1120 elements was used to produce these plots. The contour interval is 2 for $\hat{\psi}$ and 0.2 for $\hat{T}$ and $\hat{C}$. The flow consists of rising hot fluid, with a high solute concentration, in the center of the domain and colder fluid, with a lower solute concentration, sinking along the adiabatic and impermeable side walls.

buoyant and rises again. As time increases, convection and diffusion act to decrease the temperature and salinity gradients in the flow interior. At low $R\rho$, the thermal buoyancy forces eventually overwhelm the negative buoyancy forces of the salinity field and a convective steady-state with thin compositional and thermal boundary layer is reached.

For intermediate $R\rho$, convection evolves to a chaotic state in which regions of sharp temperature and salinity gradients are highly mobile in time and space. As $R\rho$ increases, a motionless brine layer forms and increases in thickness at the bottom of the domain, confining convection to the upper part of the system. The difference between the convective dynamics in the low $R\rho$ and intermediate $R\rho$ cases is illustrated in the KE phase plots and power spectra shown in Figs. 8 and 9. Figure 8(a) shows the KE phase plot for $R\rho = 0.25$. Here, the KE–$\dot{KE}$ trajectory spirals into a stable fixed point. The KE phase plot for $R\rho = 0.75$ is shown in Fig. 8(b). In this case, the KE–$\dot{KE}$ trajectory follows an irregular orbit in a loosely defined region of phase space and never reaches a fixed point. Figure 9(a) gives the KE power spectrum for $R\rho = 0.25$. This power spectrum contains a single dominant frequency along with its harmonics. The KE power spectrum for $R\rho = 0.75$ is shown in Fig. 9(b). In this case, the spectrum is characterized by broadband noise.

At high $R\rho$, convection is characterized at early time by flow confined to the upper part of the domain. The system eventually evolves to a steady-state where the velocity is zero everywhere and the temperature and salinity fields are conductive.

'Layered box'. Time-dependent simulations were performed with $R\rho$ ranging from 0 to 2 for the 'salted from below' boundary condition and the 'layered box' initial condition. For the passive tracer case ($R\rho = 0$), the composition layers rapidly break down; the steady-state field plots for this case are identical to those shown in Fig. 6. Nu time series plots for four of these simulations are given in Fig. 10.

For $R\rho = 0.25$, the initially layered salinity field also rapidly breaks down and the system evolves to a convective steady-state. At intermediate $R\rho$ values, the system is characterized at early time by oscillatory convection in each composition layer. These layers are separated by a highly mobile interface which oscillates between concave up and concave down (Fig. 11). At later time, this interface becomes highly distorted, and convection becomes chaotic. At high $R\rho$, the flow field at early time consists of vertically stacked convection cells with a nearly horizontal interface between the layers. At later time, these systems evolve to a static steady-state. This static steady-state, with stationary fluid and conductive temperature and salinity profiles, is the same steady-state reached at high $R\rho$ values for the 'empty box' initial condition. However, the transition between solutions which appear to be permanently unsteady and solutions which evolve to a static steady-state, occurs at a lower $R\rho$ value for the 'layered box' initial condition than for the 'empty box' initial condition.

'Linear box'. Finally, the 'linear box' initial condition for a system with the 'salted from below' boundary condition was considered. The dynamics of this system as a function of $R\rho$ are similar to the 'empty box' and the 'layered box' cases. The system evolves to a convective steady-state at low $R\rho$ and to a conductive steady state for high $R\rho$. At intermediate $R\rho$, the system is characterized by chaotic flows. Solutions with vertically stacked convection cells were never obtained.

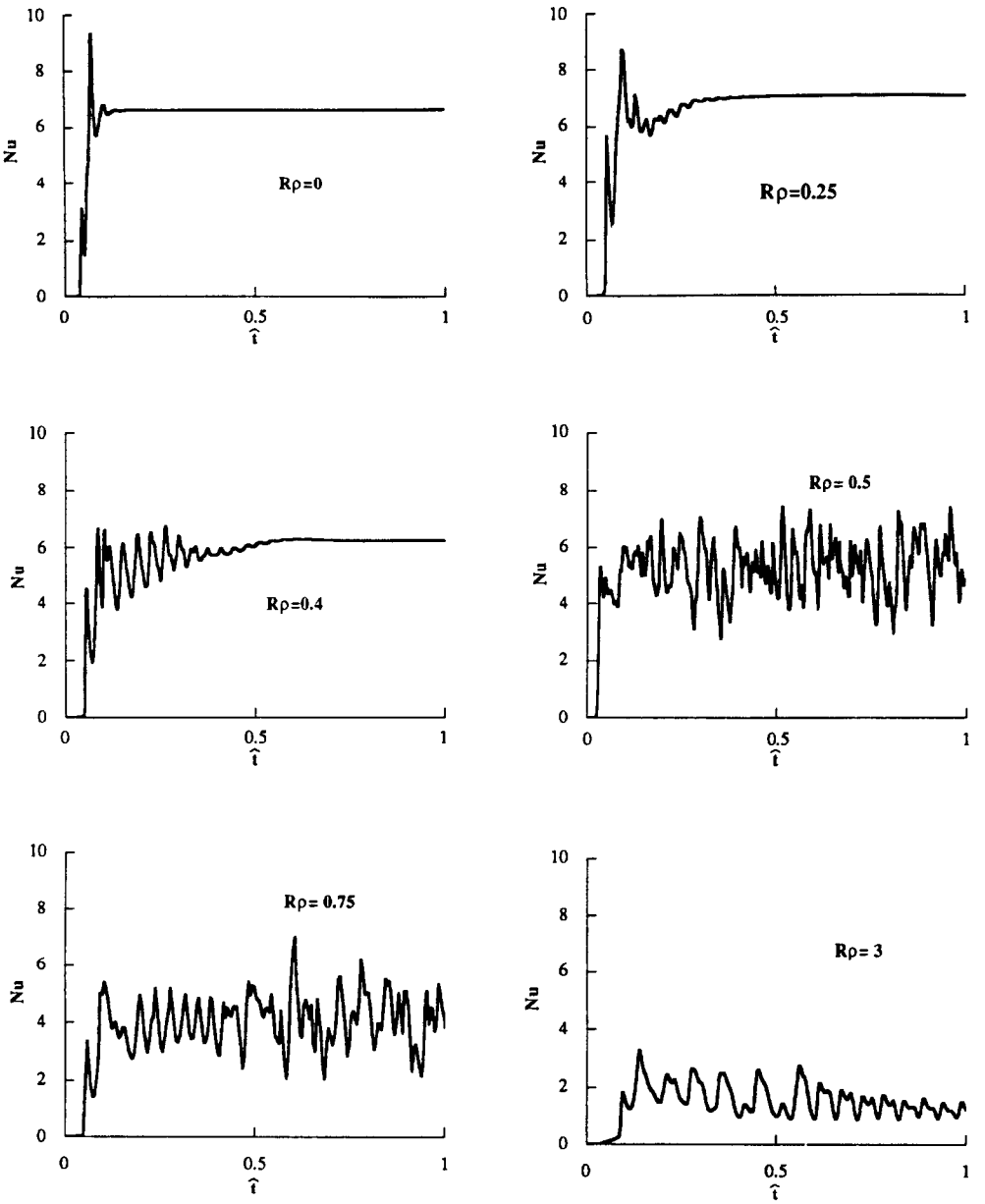

FIG. 7. *Nu* vs time plots for porous media heated from below with the 'salted from below' boundary condition and 'empty box' initial condition on composition. Simulations were performed for $R\rho$ values between 0 and 3 with $Ra = 600$, $Le = 20$, $\phi^* = 1$. For $R\rho = 0$, 0.25 and 0.4, the systems evolve to a convective steady-state. For $R\rho = 0.5$ and 0.75, the systems remain unsteady. At $R\rho = 3$, the system evolves to a conductive steady-state (with *Nu* reaching 1 at $\hat{t} > 1$).

Time-dependent — 'no flux'

Time-dependent simulations were performed with $R\rho$ ranging from 0 to 1.5 for the 'no flux' boundary condition and the 'layered box' initial condition. This is essentially a pure mixing problem. For the passive tracer case ($R\rho = 0$), the steady-state velocity and temperature field plots are identical to those shown in Fig. 6. However, the composition field at steady-state for these boundary conditions is homogeneous, unlike the composition field in Fig. 6.

As discussed above in the section on steady-state results, the convective steady-state for these boundary conditions depends on *Ra* only. The evolution to this steady-state for the 'layered box' initial condition, however, increases in complexity with increasing $R\rho$. At early time, convection is oscillatory and occurs in the form of vertically stacked cells. The interface between the two composition layers is highly mobile, oscillating between concave up and concave down, with amplitude increasing with time. Eventually the interface reaches the top or bottom of the domain, 'cracks', and the composition field rapidly homo-

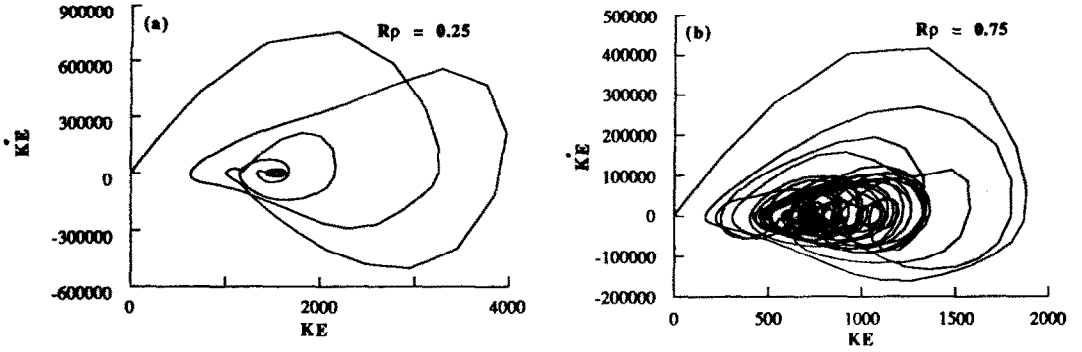

FIG. 8. *KE* phase plots showing the trajectory in *KE*–$\dot{KE}$ space for porous media heated from below with the 'salted from below' boundary condition and 'empty box' initial condition on composition. The parameters for this problem are (a) $Ra = 600$, $Le = 20$, $\phi^* = 1$ and $R\rho = 0.25$ and (b) $R\rho = 0.75$.

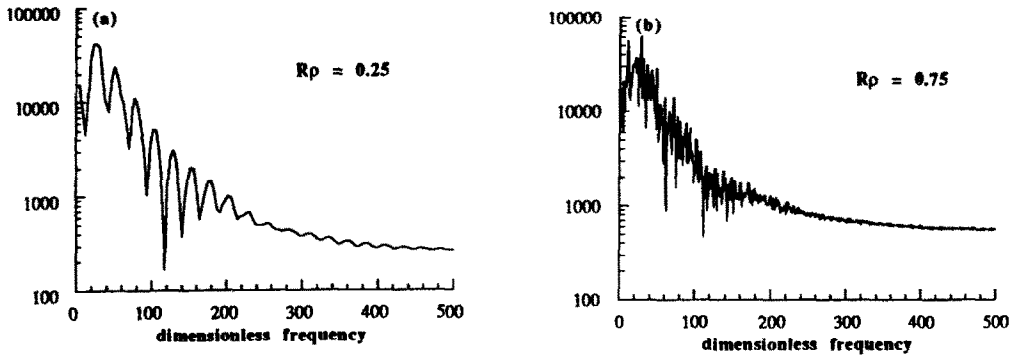

FIG. 9. *KE* power spectra for porous media heated from below with the 'salted from below' boundary condition and 'empty box' initial condition on composition. The parameters for this problem are (a) $Ra = 600$, $Le = 20$, $\phi^* = 1$ and $R\rho = 0.25$ and (b) $R\rho = 0.75$.

genizes. It is noted that Griffiths [20], in his experimental work, observed the interface between two layers with different initial temperature and chemical concentrations to be distorted and nonplanar for low $R\rho$. Finally, for $R\rho > 1$, the system evolves to a static quasi-steady-state on a thermally diffusive time scale, $\hat{t} \approx 1$ (or $t \approx H^2\sigma\kappa^{-1}$). That is, at $\hat{t} \approx 1$ the temperature and salinity fields are conductive and the velocity is zero everywhere; however, the salinity field will eventually homogenize and these systems too will evolve to a convective steady-state which is a function of Ra only. It is expected that the lifetime of the quasi-steady-state characterized by conduction is $\hat{t} \approx Le$.

CONCLUSIONS

Convective flows through porous media heated from below in a square domain with two opposing sources of buoyancy (heat and salt) have been investigated for a variety of boundary and initial conditions on the salinity field. Steady-state calculations with the 'salted from below' boundary condition in the region $100 < Ra < 600$, $10 < Le < 100$, $0 < R\rho < 0.4$ show that $Nu \propto Ra^{3/5}(1 - R\rho)^{1/2}$ and $Sh \propto Ra^{3/5}Le^{1/2}(1 - R\rho)^{1/2}$. Time-dependent simulations with $\phi^* = 1$ show that the flow dynamics depend strongly on $R\rho$. When the system is 'salted from below', the dynamics of convection for low $R\rho$ are similar to the passive tracer case. The systems evolve to a convective steady-state. The evolution to this steady-state increases in complexity with increasing $R\rho$ due to oscillations in the flow. At intermediate $R\rho$, convection is characterized by chaos. At high $R\rho$, systems evolve to a static steady-state with conductive temperature and salinity profiles. These flow dynamics are basically the same regardless of the initial conditions on the salinity field. When no salt is allowed to enter or leave the domain, the system evolves to a convective steady-state independent of $R\rho$. However, the system reaches a conductive quasi-steady-state for large $R\rho$ on a thermal diffusion time scale ($\hat{t} \approx 1$). For an initially layered composition field, for both the 'salted from below' and 'no flux' boundary conditions considered here, vertically stacked convection cells exist transiently. The interface between the layer is highly unsteady and regions of sharp temperature and salinity gradients are mobile in time and space.

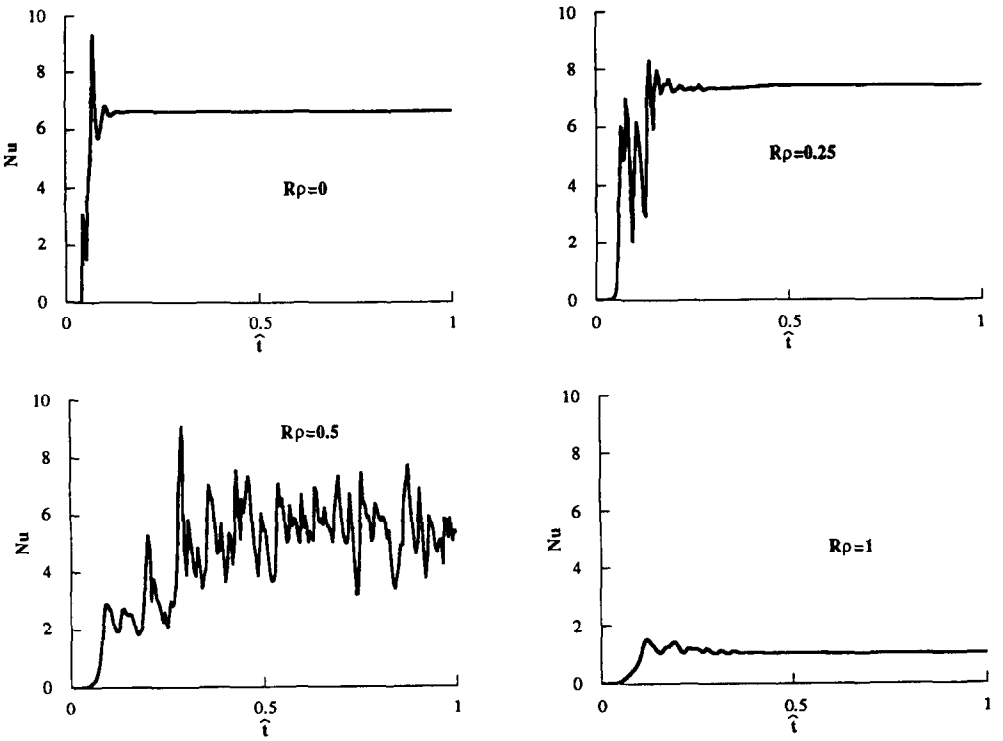

FIG. 10. *Nu* vs time plots for porous media heated from below with the 'salted from below' boundary conditions and 'layered box' initial condition on composition. Simulations were performed for various $R\rho$ values with $Ra = 600$, $Le = 20$, $\phi^* = 1$. For $R\rho = 0$ and 0.25, the systems evolve to a convective steady-state. For $R\rho = 0.5$, the system remains unsteady. At $R\rho = 1$, the system evolves to a conductive steady-state with $Nu = 1$.

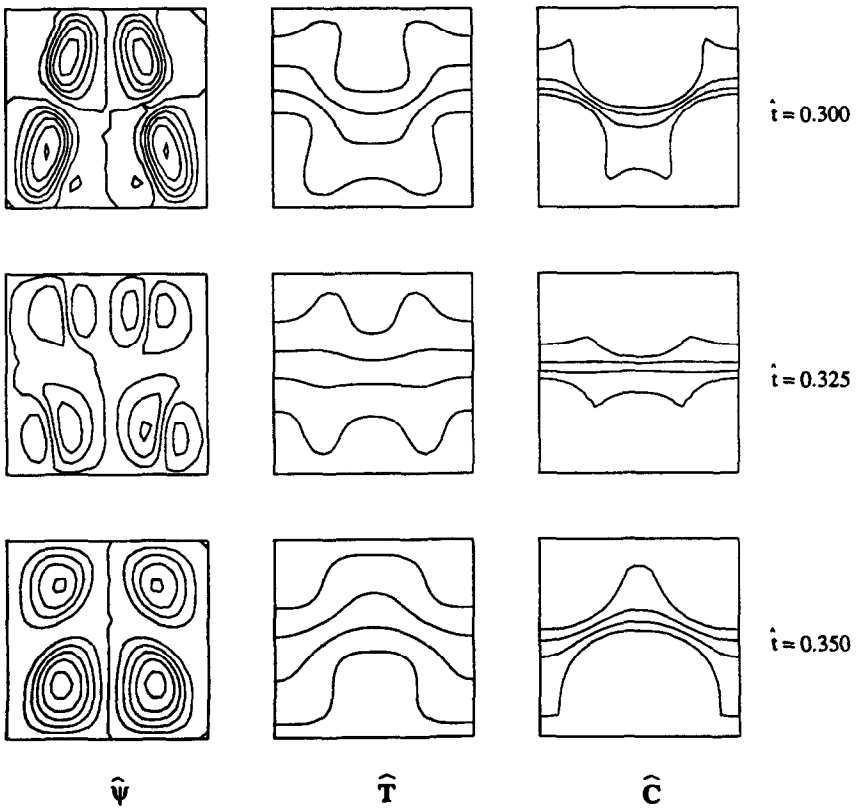

FIG. 11. (a) Velocity, (b) temperature and (c) salinity field plots at $\hat{t} = 0.3$–0.35 for porous media heated from below with the 'salted from below' boundary condition and 'layered box' initial condition on composition. The parameters for this problem are $Ra = 600$, $Le = 20$, $\phi^* = 1$ and $R\rho = 0.75$. The contour interval is 2 for $\hat{\psi}$ and 0.2 for $\hat{T}$ and $\hat{C}$. The composition layers are separated by a highly mobile interface.

This study suggests that double-diffusive convection may indeed occur in natural hydrothermal systems. In systems with relatively low chemical buoyancy, convection with very thin chemical boundary layers at the top and bottom of the systems may exist; the interior of the system would be homogeneous. The chaotic numerical simulations reported here suggest that temperature and salinity may vary greatly in both time and space in natural systems. Additional studies which explicitly consider the role of porosity, ϕ, are now in progress.

Acknowledgement—NDR acknowledges financial support from Associated Western Universities in the form of a graduate fellowship. Computations were performed at the San Diego Supercomputer Center and NASA Ames Research Center. This research is supported by NSF OCE89-11396 to FJS and R. Haymon.

REFERENCES

1. M. Combarnous and S. Bories, Natural convection in saturated porous media, *Adv. Hydroscience* **10,** 231–307 (1975).
2. P. Cheng, Heat transfer in geothermal systems, *Adv. Heat Transfer* **14,** 1–105 (1978).
3. J. S. Turner, Multicomponent convection, *Ann. Rev. Fluid Mech.* **17,** 11–44 (1985).
4. L. M. Cathles, Scales and effects of fluid flow in the upper crust, *Science* **248,** 323–329 (1990).
5. H. C. Helgeson, Geologic and thermodynamic characteristics of the Salton Sea geothermal system, *Am. J. Sci.* **266,** 129–166 (1968).
6. R. O. Fournier, Double-diffusive convection in geothermal systems: the Salton Sea, California, geothermal system as a likely candidate, *Geothermics* **19,** 481–496 (1990).
7. D. A. Nield, Onset of thermohaline convection in a porous medium, *Water Resources Res.* **4,** 553–560 (1968).
8. J. W. Taunton, E. N. Lightfoot and T. Green, Thermohaline instability and salt fingers in a porous medium, *Physics Fluids* **15,** 748–753 (1972).
9. H. Rubin, Effect of solute dispersion on thermal convection in a porous medium layer, 2, *Water Resources Res.* **11,** 154–158 (1975).
10. H. Rubin, Effect of solute dispersion on thermal convection in a porous medium layer, *Water Resources Res.* **9,** 968–974 (1973).
11. P. A. Tyvand, Thermohaline instability in anisotropic porous media, *Water Resources Res.* **16,** 325–330 (1980).
12. N. Rudraiah, P. K. Srimani and R. Friedrich, Finite amplitude convection in a two-component fluid saturated porous layer, *Int. J. Heat Mass Transfer* **25,** 715–722 (1981).
13. D. Poulikakos, Double-diffusive convection in horizontal sparsely packed porous layer, *Int. Commun. Heat Mass Transfer* **13,** 587–598 (1986).
14. M. E. Taslim and U. Narusaw, Binary fluid composition and double-diffusive convection in a porous medium, *J. Heat Transfer* **108,** 221–224 (1986).
15. O. V. Trevisan and A. Bejan, Natural convection with combined heat and mass transfer buoyancy effects in a porous medium, *Int. J. Heat Mass Transfer* **28,** 1597–1611 (1985).
16. K. N. Mehta and K. Nandakuma, Natural convection with combined heat and mass transfer buoyancy effects in a non-homogeneous porous medium, *Int. J. Heat Mass Transfer* **30,** 2651–2656 (1987).
17. Z. Zhang and A. Bejan, The horizontal spreading of thermal and chemical deposits in a porous medium, *Int. J. Heat Mass Transfer* **30,** 2289–2303 (1987).
18. O. V. Trevisan and A. Bejan, Mass and heat transfer by high Rayleigh number convection in a porous medium heated from below, *Int. J. Heat Mass Transfer* **30,** 2341–2356 (1987).
19. B. T. Murray and C. F. Chen, Double-diffusive convection in a porous medium, *J. Fluid Mech.* **201,** 147–166 (1989).
20. R. W. Griffiths, Layered double-diffusive convection in porous media, *J. Fluid Mech.* **102,** 221–248 (1981).
21. O. V. Trevisan and A. Bejan, Combined heat and mass transfer by natural convection in a porous medium, *Adv. Heat Transfer* **20,** 314–352 (1990).
22. J. Bear, *The Dynamics of Fluids in Porous Media.* Dover, New York (1972).
23. C. M. Oldenburg, F. J. Spera, D. A. Yuen and G. Sewell, Dynamic mixing in magma bodies: theory simulations, and implications, *J. Geophys. Res.* **94,** 9215–9236 (1989).
24. N. D. Rosenberg and F. J. Spera, Role of anisotropic and/or layered permeability in hydrothermal systems, *Geophys. Res. Lett.* **17,** 235–238 (1990).
25. G. Sewell, *Analysis of a Finite Element Method: PDE/PROTRAN.* Springer, New York (1985).
26. J. Caltagirone, Thermoconvective instabilities in a horizontal porous layer, *J. Fluid Mech.* **72,** 269–287 (1975).
27. G. Schubert and J. M. Straus, Three-dimensional and multicellular steady and unsteady convection in fluid-saturated porous media at high Rayleigh numbers, *J. Fluid Mech.* **94,** 25–38 (1979).
28. T. Kaneko, M. F. Mohtadi and K. Aziz, An experimental study of natural convection in inclined porous media, *Int. J. Heat Mass Transfer* **17,** 485–496 (1974).
29. F. J. Buretta and A. S. Berman, Convective heat transfer in a liquid saturated porous layer, *J. Appl. Mech.* **98,** 249–253 (1976).
30. J. W. Elder, Steady free convection in a porous medium heated from below, *J. Fluid Mech.* **27,** 229–248 (1967).

CONVECTION THERMOHALINE DANS UN MILIEU POREUX CHAUFFE PAR LE BAS

Résumé—On présente des résultats sur des calculs numériques de convection dans les milieux poreux chauffés par le bas, avec deux sources opposées de flottement (chaleur et salinité). Les calculs de régime permanent avec une condition de composition "salée par le bas" aux limites et de Dirichlet pour la température, dans la région $100 < Ra < 600$, $10 < Le < 100$, $0 < R\rho < 0{,}4$, montrent que $Nu \propto Ra^{3/5}(1-R\rho)^{1/2}$ et $Sh \propto Ra^{3/5}Le^{1/2}(1-R\rho)^{1/2}$. Des simulations dépendent fortement de $R\rho$ pour Ra et Le constants. Quand le système est "salé par le bas", le changement dynamique avec $R\rho$ croissant pour un système évolue d'un état permanent convectif bien mélangé jusqu'à un autre dans lequel l'écoulement est chaotique avec des fluctuations à large amplitude dans la composition, et finalement à un autre qui mène à un état conductif permanent. Pour du champ de salinité initialement stratifié, des cellules de convection verticalement empilées peut exister temporairement; l'interface entre les couches est extrêmement instable.

THERMISCH UND KONZENTRATIONSGETRIEBENE KONVEKTION IN EINEM VON UNTEN BEHEIZTEN PORÖSEN MEDIUM

Zusammenfassung—Es wird über die Ergebnisse einer numerischen Untersuchung der Konvektion in einem von unten beheizten porösen Medium berichtet, wobei es zwei gegengerichtet wirkende Ursachen für Auftrieb gibt (beispielsweise Wärme und Salzgehalt). Für folgende Randbedingungen werden stationäre Berechnungen ausgeführt: Es erfolgt eine Salzzufuhr von unten, und für die Temperatur wird die Dirichlet-Bedingung angewandt. Die Untersuchungen im Bereich $100 < Ra < 600$, $10 < Le < 100$, $0 < R\rho < 0{,}4$ ergaben folgende Zusammenhänge: $Nu \propto Ra^{3/5}(1-R\rho)^{1/2}$ sowie $Sh \propto Ra^{3/5}\ Le^{1/2}(1-R\rho)^{1/2}$. Die zeitabhängigen Simulationsrechnungen zeigen, daß die Strömung bei konstanten Werten von Ra und Le sehr stark von $R\rho$ abhängt. Bei einer Salzzufuhr von unten ändert sich das dynamische Verhalten des Systems mit zunehmenden Werten von $R\rho$: Die Entwicklung führt zunächst zu einem stationären Zustand mit Mischkonvektion, dann zu einer chaotischen Strömung mit großen Fluktuationen in der Gemischzusammensetzung und schließlich zu einem stationären Zustand mit reiner Leitung. Für den Fall einer anfänglich geschichteten Salzverteilung können vorübergehend senkrecht übereinandergeschichtete Konvektionszellen auftreten. Die Grenzfläche zwischen den Schichten ist äußerst instationär.

ТЕРМОГАЛИННАЯ КОНВЕКЦИЯ В НАГРЕВАЕМОЙ СНИЗУ ПОРИСТОЙ СРЕДЕ

Аннотация—Приводятся результаты численных экспериментов по конвекции в нагреваемой снизу пористой среде при наличии температурной и концентрационной неоднородностей, действующих в противоположных направлениях. Расчеты в стационарном случае при наложении граничного условия с "соленостью снизу" и условий Дирихле для температуры в области $100 < Ra < 600$, $10 < Le < 100$, $0 < R\rho < 0{,}4$ показывают, что $Nu \propto Ra^{3/5}(1 - R\rho)^{1/2}$ и $Sh \propto Ra^{3/5}Le^{1/2}(1 - R\rho)^{1/2}$. Нестационарное моделирование выявляет существенную зависимость течений от значения $R\rho$ при постоянных значениях Ra и Le. При наложении на систему условия "солености снизу" с ростом значения $R\rho$ происходит переход от хорошо перемешанного конвективного устойчивого состояния к состоянию, когда течение является хаотическим с большими амплитудными колебаниями состава и, наконец, к состоянию, развивающемуся в кондуктивное устойчивое. В условиях первоначального расслоения поля солености вертикально расположенные ячейки конвекции могут находиться в нестационарном состоянии и граница раздела между слоями является крайне неустойчивой.